

# Causal Flow-based Variational Auto-Encoder for Disentangled Causal Representation Learning

Di Fan, Yannian Kou, Chuanhou Gao\*

---

## Abstract

Disentangled representation learning aims to learn low-dimensional representations of data, where each dimension corresponds to an underlying generative factor. Currently, Variational Auto-Encoder (VAE) are widely used for disentangled representation learning, with the majority of methods assuming independence among generative factors. However, in real-world scenarios, generative factors typically exhibit complex causal relationships. We thus design a new VAE-based framework named Disentangled Causal Variational Auto-Encoder (DCVAE), which includes a variant of autoregressive flows known as causal flows, capable of learning effective causal disentangled representations. We provide a theoretical analysis of the disentanglement identifiability of DCVAE, ensuring that our model can effectively learn causal disentangled representations. The performance of DCVAE is evaluated on both synthetic and real-world datasets, demonstrating its outstanding capability in achieving causal disentanglement and performing intervention experiments. Moreover, DCVAE exhibits remarkable performance on downstream tasks and has the potential to learn the true causal structure among factors.

*Keywords:*

variational auto-encoder, disentangled representation learning

---

## 1. Introduction

Representation learning aims to learn data representations that simplify information extraction for constructing classifiers or predictors [1]. Disentangled representation learning is an important step towards better representation learning. It aims to learn factorized representations that can effectively identify and disentangle the latent factors in observed data [2]. Due to its capability of generating robust and interpretable representations, disentangled representation learning has become crucial in various domains, such as computer vision and recommendation systems [3–10].

One of the most commonly utilized frameworks for learning disentangled representations is the Variational Auto-Encoder

(VAE) [11], which has gained considerable popularity [12–15]. The primary focus of the research involves imposing independent constraints on the posterior or aggregated posterior of latent variables  $z$  through KL divergence [16–22]. However, they all made the assumption that the generative factors are independent of each other. Yet, in reality, the generative factors of interest are likely to have causal relationships with each other. For example, in a human face image dataset, when considering the generative factors for generating faces, such as factors like opening the mouth and smiling, a causal relationship between them becomes apparent. When an individual is smiling, there's a greater probability of maintaining an open-mouth state. Here, smiling functions as a causal variable, while opening the mouth acts as an effect variable. In this scenario, the models mentioned earlier encounter difficulties in learning the disentangled representations [23]. To tackle this issue, recent state-of-the-art methods have shifted their focus towards causal disentangled

---

\*Corresponding author

*Email addresses:* fandi@zju.edu.cn (Di Fan),

kouyannian@zju.edu.cn (Yannian Kou), gaouchou@zju.edu.cn

(Chuanhou Gao)

representation learning [24–32]. These methods either rely on existing Structural Causal Models (SCMs) to introduce causal relationships or focus solely on modeling the causal structure of generative factors in specific scenarios. On the contrary, we explore the integration of causal relationships into the model by utilizing normalization flows, a technique recently developed in the deep learning literature, eliminating the necessity on pre-existing SCMs.

Normalizing flows [33] present a general approach for constructing generative models. They ensure both efficient and accurate sampling as well as density estimation. Recently, normalization flows have become prevalent in the context of utilizing VAE. They enhance the inference capability of VAE by approximating the posterior distribution more closely to reality [34]. As one of the most widely used types within the normalization flow framework, autoregressive normalization flows are favored in VAE due to their ability to generate triangular Jacobian matrices [35, 36]. Notably, autoregressive flows have demonstrated potential in learning causal orders between two variables or pairs of multivariate variables from a dataset [37]. However, their primary focus has been solely on causal discovery tasks. Wehenkel and Louppe [38] introduced a graphical normalizing flow, incorporating a conditioner that utilizes an adjacency matrix. They investigated the relationship between different flows from a Bayesian network perspective and designed the model for improved density estimation, but with no specific focus on achieving causal disentangled representations. Inspired by these applications, we have developed causal flows based on autoregressive flows, which can endow variables with causal structural information about the true generating factors. At this point, causal flows not only inherit the advantages of traditional autoregressive flows combined with VAE to enhance VAE’s inference ability, but on the other hand, they incorporate the factor information by leveraging the structural characteristics of flow models. Consequently, they help VAE in learning causal disentangled representations during the inference process, representing the first use of flow models in this field.

In this paper, we first introduce causal flows to integrate

information about causal relationships among generative factors. Then, we present a novel VAE-based framework named Disentangled Causal Variational Auto-Encoder (DCVAE), which merges VAE with causal flows to effectively learn causal disentangled representations. After encoding the input data with DCVAE’s encoder and processing it through causal flows, we obtain the causal disentangled representations. These representations are then fed into the decoder for the reconstruction of the original images. To enhance the flexibility of the prior distribution in DCVAE, we further introduce the conditional prior. Additionally, we incorporate the regularization term into the loss function of DCVAE to theoretically ensure causal disentanglement. The main contributions can be summarized as follows:

- a) We introduce causal flows, the improved autoregressive flows that can integrate causal structure information of ground-truth factors to enhance representations expressiveness.
- b) We propose a new VAE-based framework, Disentangled Causal Variational Auto-Encoder (DCVAE). We theoretically prove that DCVAE satisfies disentanglement identifiability, ensuring that our model has the capacity to learn causal disentangled representations.
- c) To validate the effectiveness of our proposed model, we conduct comprehensive experiments on both synthetic and real-world datasets. The results demonstrate that DCVAE successfully generates representations with causal semantics, achieving causal disentanglement and performing well in intervention experiments, including the generation of counterfactual images. Our model further exhibits excellent performance in terms of sampling efficiency and distributional robustness in downstream tasks.

In the rest of the paper, we start by discussing related works in Section 2 and then introduce preliminaries in Section 3. Section 4 describes our proposed causal flows, and Section 5 presents the overall framework of our model, DCVAE, including the objective function and theoretical proof of the model’s ability to learn disentangled representations. In Section 6, we present both quantitative and qualitative experiments, offering a

comprehensive evaluation of our model’s performance. Finally, the conclusion in Section 7 highlights the innovation of our approach and suggests potential directions for future research.

## 2. Related Work

### 2.1. Disentangled Representation Learning

Disentangled representation learning aims to disentangle latent explanatory factors behind the observed data [1]. It assumes that high dimensional data is generated by low-dimensional, semantically meaningful generative factors, which are called ground-truth factors. Thus, a disentangled representation is characterized by changes in one dimension being solely caused by one factor of variation in the data. This pursuit, endowed with the ability to generate robust, controllable, and interpretable representations, has emerged as a challenging issue in machine learning.

Generally, variational methods are widely employed for disentangled representation in images, utilizing an encoder-decoder framework to learn mutually independent latent factors. The variational approach employs a standard normal distribution as the prior for latent variables and then uses the variational posterior to approximate the unknown true posterior. By introducing new independent regularization terms into the original loss function, this framework is further extended, giving rise to various algorithms [16–22, 39].  $\beta$ -VAE [16] imposed a greater weight ( $\beta > 1$ ) on the KL divergence between the variational posterior and prior to employ a modified version of the VAE objective. In  $\beta$ -TCVAE [19], a total correlation penalty was incorporated into the objective to encourage the model to identify statistically independent factors in the data distribution. DIP-VAE [20] introduced a regularizer on the expectation of the approximate posterior over observed data, promoting disentanglement. Unfortunately, Locatello et al. [2] showed that the unsupervised learning of disentangled representations is theoretically impossible from observations without inductive biases. Therefore, several weakly supervised or supervised methods were proposed.[40–43]. For instance, Locatello et al. [43] explored the task of learning disentangled representations from

pairs of non-i.i.d. observations, where these observations share an unknown, random subset of factors of variation. They also investigated the impact of different supervision modalities. Furthermore, Khemakhem et al. [44] introduced a conditional VAE, assuming that latent variables are conditionally independent given some additionally observed variables. The latent variable model they proposed, particularly VAE, generated a provable disentangled representation under appropriate conditions.

However, the most popular existing methods for disentanglement fail to effectively learn disentangled representations for data with strongly correlated factors, a scenario commonly encountered in real-world situations [23, 24].

### 2.2. Causal Representation Learning

Recognizing the limitations of the aforementioned methods in addressing general scenarios, there has been a growing interest in achieving causal disentangled representations through VAE. Nevertheless, the exploration of related methods still remains relatively limited.

Schölkopf [45] emphasized the importance of causal disentangled representations, providing a conceptual introduction. The disentangled causal mechanisms investigated in Suter et al. [26] and Reddy et al. [27] assumed that the underlying factors are conditionally independent given a shared confounder. This imposes strict constraints on the latent structure of the generative factors, excluding cases where the real factors may have causal effects on each other. For models that do not constrain the causal graph among generative factors, supervised methods are commonly employed. Yang et al. [25] designed an SCM layer to model the causal generative mechanisms of data. Building upon iVAE [44], they adopted a conditional prior given the ground-truth factors, thus operating in a fully supervised setting. Similarly, DEAR [24] utilized an SCM to construct the prior distribution in a weakly supervised manner. In our work, we also utilize the labels of the concepts as supervision signals. We believe this supervised approach is feasible and applicable to real-world datasets. For instance, in the case of real human-face datasets, the features we are interested in are readily extractable

from the raw data, such as gender and smiling status.

Other models also impose structure on the latent space of VAEs. For instance, Graph VAE [46] applied a chained structure in the latent space and imposed a structural causal model (SCM) on the latent space of VAE. However, the primary motivation behind Graph VAE is to enhance the expressive power of VAE rather than specifically focusing on disentangling latent causal factors. Subsequently, An et al. [28] proposed that training a disentangled decoder is essential. There are other methods for learning causal disentangled representations, extending beyond generative models like VAE [26, 45, 47]. However, in comparison to our model, which leverages causal flows within VAE, their model structures differ significantly from ours.

Relatively speaking, our proposed model considers general scenarios where generative factors can exhibit more complex causal relationships. Furthermore, unlike methods based on SCM, we leverage the characteristics of flow models to achieve disentanglement. This approach not only utilizes the strong fitting ability of flow models but also leverages the performance of SCMs. In other words, it integrates causal information while enhancing the expressive capacity of the inference model in VAE. Finally, it is important to emphasize that our primary focus is on representation learning, with an emphasis on the disentangled representations generated by the encoder. To the best of our knowledge, our model is the first among all VAE-based models that achieves causal disentanglement without relying on complex SCMs. Moreover, it successfully learns causal disentangled representations without imposing restrictions on the causal graph of factors.

### 3. Preliminaries

#### 3.1. Variational Auto-Encoder

Let  $\{\mathbf{x}^{(j)}\}_{j=1}^N$  denote i.i.d training data,  $\mathbf{x} \in \mathbb{R}^n$  be the observed variables and  $\mathbf{z} \in \mathbb{R}^d$  be the latent variables. The dataset  $\mathcal{X}$  has an empirical data distribution denoted as  $q_{\mathcal{X}}$ . The *generative model* defined over  $\mathbf{x}$  and  $\mathbf{z}$  is  $p_{\theta}(\mathbf{x}, \mathbf{z}) = p(\mathbf{z})p_{\theta}(\mathbf{x}|\mathbf{z})$ , where  $\theta$  is the parameter of the *decoder*. Typically,  $p(\mathbf{z}) =$

$\mathcal{N}(\mathbf{0}, \mathbf{I})$ ,  $p_{\theta}(\mathbf{x}|\mathbf{z}) = \mathcal{N}(f_{\theta}(\mathbf{z}), \sigma^2\mathbf{I})$ , where  $f_{\theta}(\mathbf{z})$  is a neural network. The marginal likelihood  $p_{\theta}(\mathbf{x}) = \int p_{\theta}(\mathbf{x}, \mathbf{z})d\mathbf{z}$  is intractable to maximize. Therefore, VAE [11] introduces a parametric *encoder*  $q_{\phi}(\mathbf{z}|\mathbf{x}) = \mathcal{N}(\mu_{\phi}(\mathbf{x}), \text{diag}(\sigma_{\phi}^2(\mathbf{x})))$ , also called an *inference model*, to obtain the variational lower bound on the marginal log-likelihood, i.e., the Evidence Lower Bound (ELBO):

$$\begin{aligned} \text{ELBO}(\phi, \theta) &= \mathbb{E}_{q_{\mathcal{X}}} [\log p_{\theta}(\mathbf{x}) - D_{\text{KL}}(q_{\phi}(\mathbf{z}|\mathbf{x})||p_{\theta}(\mathbf{z}|\mathbf{x}))] \\ &= \mathbb{E}_{q_{\mathcal{X}}} [\mathbb{E}_{q_{\phi}(\mathbf{z}|\mathbf{x})} (\log p_{\theta}(\mathbf{x}, \mathbf{z}) - \log q_{\phi}(\mathbf{z}|\mathbf{x}))] \\ &= \mathbb{E}_{q_{\mathcal{X}}} [\mathbb{E}_{q_{\phi}(\mathbf{z}|\mathbf{x})} \log p_{\theta}(\mathbf{x}|\mathbf{z}) - D_{\text{KL}}(q_{\phi}(\mathbf{z}|\mathbf{x})||p(\mathbf{z}))] \end{aligned} \quad (1)$$

As can be seen from Eq. (1), maximizing ELBO( $\phi, \theta$ ) will simultaneously maximize  $\log p_{\theta}(\mathbf{x})$  and minimize the KL divergence  $D_{\text{KL}}(q_{\phi}(\mathbf{z}|\mathbf{x})||p_{\theta}(\mathbf{z}|\mathbf{x})) \geq 0$ . Therefore, we wish  $q_{\phi}(\mathbf{z}|\mathbf{x})$  to be flexible enough to match the true posterior  $p_{\theta}(\mathbf{z}|\mathbf{x})$ . At the same time, based on the third line of Eq. (1), which is often used as objective function of VAE, we require that  $q_{\phi}(\mathbf{z}|\mathbf{x})$  is efficiently computable, differentiable, and sampled from.

#### 3.2. Autoregressive Normalizing Flows

*Normalizing flows* [34] are effective solutions to the issues mentioned above. The flows construct flexible posterior distribution through expressing  $q_{\phi}(\mathbf{z}|\mathbf{x})$  as an expressive invertible and differentiable mapping  $\mathbf{g}$  of a random variable with a relatively simple distribution, such as an isotropic normal. Typically,  $\mathbf{g}$  is obtained by composing a sequence of invertible and differentiable transformations  $\mathbf{g}^{(1)}, \mathbf{g}^{(2)}, \dots, \mathbf{g}^{(K)}$ , i.e.,  $\mathbf{g} = \mathbf{g}^{(K)} \circ \dots \circ \mathbf{g}^{(1)}, \mathbf{g}^{(k)} : \mathbb{R}^{d+n} \rightarrow \mathbb{R}^d, \forall k = 1 \dots K$ . If we define the initial random variable (the output of encoder) as  $\mathbf{z}^{(0)}$  and the final output random variable as  $\mathbf{z}^{(K)}$ , then  $\mathbf{z}^{(k)} = \mathbf{g}^{(k)}(\mathbf{z}^{(k-1)}, \mathbf{x}), \forall k$ . In this case, we can use  $\mathbf{g}$  to obtain the conditional probability density function of  $\mathbf{z}^{(K)}$  by applying the general probability-transformation formula [33]:

$$q_{\phi}(\mathbf{z}^{(K)}|\mathbf{x}) = q_{\phi}(\mathbf{z}^{(0)}|\mathbf{x}) |\det J_{\mathbf{g}(\mathbf{z}^{(0)}, \mathbf{x})}| \quad (2)$$

where  $\det J_{\mathbf{g}(\mathbf{z}^{(0)}, \mathbf{x})}$  is the Jacobian determinant of  $\mathbf{g}$  with respect to  $\mathbf{z}^{(0)}$ .

*Autoregressive flows* are one of the most popular normalizing flows [33, 35, 36]. By carefully designing the function  $g$ , the Jacobian matrix in Eq. (2) becomes a lower triangular matrix. For illustration, we will only use a single-step flow with notation  $g$ . Multi-layer flows are simply the composition of the function represented by a single-step flow, as mentioned earlier. And we will denote the input to the function  $g$  as  $\mathbf{z}$  and its output as  $\tilde{\mathbf{z}}$ . In the autoregressive flows,  $g$  has the following form:

$$\tilde{\mathbf{z}} = \mathbf{g}(\mathbf{z}, \mathbf{x}) = [g_1(\mathbf{z}_1; \mathbf{h}_1) \dots g_d(\mathbf{z}_d; \mathbf{h}_d)]^T \quad (3)$$

where  $\mathbf{h}_i = \mathbf{c}_i(\tilde{\mathbf{z}}_{<i}, \mathbf{x})$

where  $g_i$ , an invertible function of input  $\mathbf{z}_i$ , is termed as a **transformer**. Here  $\mathbf{z}_i$  stands for the  $i$ -th element of vector  $\mathbf{z}$ , and  $\mathbf{c}_i$  is the  $i$ -th **conditioner**, a function of the first  $i - 1$  elements of  $\tilde{\mathbf{z}}$ , which determines part of parameters of the transformer  $g_i$ . We use neural networks to fit  $c$ .

#### 4. Causal Flows

In this section, we propose an extension to the autoregressive flows by incorporating an adjacency matrix  $A$ . The extended flows still involve functions with tractable Jacobian determinants.

In autoregressive flows, causal order is established among variables  $\tilde{\mathbf{z}}_1, \dots, \tilde{\mathbf{z}}_d$ . Given the causal graph of the variables  $\tilde{\mathbf{z}}_1, \dots, \tilde{\mathbf{z}}_d$ , let  $A \in \mathbb{R}^{d \times d}$  denote its corresponding binary adjacency matrix,  $A_{i,:}$  is the row vector of  $A$  and  $A_{i,j}$  is nonzero only if  $\tilde{\mathbf{z}}_j$  is the parent node of  $\tilde{\mathbf{z}}_i$ , then  $A$  corresponding to the causal order in autoregressive flows is a full lower-triangular matrix. The conditioner can be written in the form of  $\mathbf{c}_i(\tilde{\mathbf{z}} \circ A, \mathbf{x})$ , where  $\circ$  is the element-wise product. If we utilize prior knowledge about the true causal structure among variables, i.e., if a certain causal structure among variables is known, then  $A$  is still a lower triangular matrix, but some of its entries are set to 0. We can integrate such  $A$  into the conditioner to include causal structure information in the model, which is also denoted as  $\mathbf{c}_i(\tilde{\mathbf{z}} \circ A, \mathbf{x})$ . We will refer to it as the **causal conditioner** in the following.

We define autoregressive flows that use the causal conditioner as **Causal Flows**. The transformer can be any invertible

function, and we focus on affine transformer, which is one of the simplest transformers. Therefore, causal flows  $g$  can be formulated as follows:

$$\tilde{\mathbf{z}}_i = g_i(\mathbf{z}_i; \mathbf{h}_i) = \mathbf{z}_i \exp(s_i(\tilde{\mathbf{z}} \circ A_{i,:}, \mathbf{x})) + t_i(\tilde{\mathbf{z}} \circ A_{i,:}, \mathbf{x}) \quad (4)$$

where  $\mathbf{s} = [s_1, \dots, s_d]^T \in \mathbb{R}^d$  and  $\mathbf{t} = [t_1, \dots, t_d]^T \in \mathbb{R}^d$  are defined by the conditioner, i.e.,  $\mathbf{h}_i = \{s_i, t_i\}$ , and  $s_1$  and  $t_1$  are constants.

Given that the derivative of the transformer with respect to  $\mathbf{z}_i$  is  $\exp(s_i(\tilde{\mathbf{z}} \circ A_{i,:}, \mathbf{x}))$  and  $A$  is lower-triangular, the log absolute Jacobian determinant is:

$$\log |\det J_{\mathbf{g}(\mathbf{z}, \mathbf{x})}| = \sum_{i=1}^d \log \exp(s_i(\tilde{\mathbf{z}} \circ A_{i,:}, \mathbf{x})) \quad (5)$$

$$= \sum_{i=1}^d s_i(\tilde{\mathbf{z}} \circ A_{i,:}, \mathbf{x}) \quad (6)$$

Now, we are able to derive the log probability density function of  $\tilde{\mathbf{z}}$  using the following expression:

$$\log q_{\phi}(\tilde{\mathbf{z}}|\mathbf{x}) = \log q_{\phi}(\mathbf{z}|\mathbf{x}) - \sum_{i=1}^d s_i(\tilde{\mathbf{z}} \circ A_{i,:}, \mathbf{x}) \quad (7)$$

Causal flows will not only empower our model to incorporate causal structure information but also, through the utilization of flow model characteristics, enhance the expressive capacity of the learned representations. This augmentation, consequently, enriches the information encoded in the learned representations, thereby improving the overall proficiency of our model.

It is worth noting that the computation of autoregressive flows in Eq. (3) needs to be performed sequentially, meaning that  $\tilde{\mathbf{z}}_{<i}$  must be calculated before  $\tilde{\mathbf{z}}_i$ . Due to the sampling requirement in VAE, this approach may not be computationally efficient. However, in causal disentanglement applications of VAE, the number of factors of interest is often relatively small. Additionally, we've found that using a single layer of causal flows and lower-dimensional latent variables is enough to lead to better results, so the computational cost of the model is not significantly affected by sequential sampling.

## 5. The Proposed model

This section focuses on addressing the issue of causal disentanglement in VAE. First, we introduce some notations. We denote  $\boldsymbol{\xi} \in \mathbb{R}^m$  as the underlying ground-truth factors of interest for data  $\mathbf{x}$ , with distribution  $p_{\boldsymbol{\xi}}$ . For each underlying factor  $\xi_i$ , we denote  $\mathbf{y}_i$  as some continuous or discrete annotated observation satisfying  $\xi_i = \mathbb{E}(\mathbf{y}_i|\mathbf{x})$ , where the superscript  $i$  still denotes the  $i$ -th element of each vector. Let  $\mathcal{D} = \{(\mathbf{x}^{(j)}, \mathbf{y}^{(j)}, \mathbf{u}^{(j)})\}_{j=1}^N$  denotes a labeled dataset, where  $\mathbf{u}^{(j)} \in \mathbb{R}^k$  is the additional observed variable. Depending on the context, the variable  $\mathbf{u}$  can take on various meanings, such as serving as the time index in a time series, a class label, or another variable that is observed concurrently [48]. We get  $\xi_i = \mathbb{E}(\mathbf{y}_i|\mathbf{x}, \mathbf{u})$ , where  $i = 1, \dots, m$ . This is because if  $\mathbf{u}$  is ground-truth factor  $\mathbf{y}$ , it is obviously true, otherwise,  $\xi_i = \mathbb{E}(\mathbf{y}_i|\mathbf{x}, \mathbf{u}) = \mathbb{E}(\mathbf{y}_i|\mathbf{x})$ . We will view the encoder and flows as an unified stochastic transformation  $E$ , with the learned representation  $\tilde{\mathbf{z}}$  as its final output, i.e.,  $\tilde{\mathbf{z}} = E(\mathbf{x}, \mathbf{u})$ . Additionally, in the stochastic transformation  $E(\mathbf{x}, \mathbf{u})$ , we use  $\bar{E}(\mathbf{x}, \mathbf{u})$  to denote its deterministic part, i.e.,  $\bar{E}(\mathbf{x}, \mathbf{u}) = \mathbb{E}(E(\mathbf{x}, \mathbf{u})|\mathbf{x}, \mathbf{u})$ .

Now, we adopt the definition of causal disentanglement as follows:

**Definition 1 (Disentangled representation [24]).** Considering the underlying factor  $\boldsymbol{\xi} \in \mathbb{R}^m$  of data  $\mathbf{x}$ ,  $E$  is said to learn a disentangled representation with respect to  $\boldsymbol{\xi}$  if there exists a one-to-one function  $r_i$  such that  $\bar{E}(\mathbf{x}, \mathbf{u})_i = r_i(\xi_i), \forall i = 1, \dots, m$ .

The purpose of this definition is to guarantee some degree of alignment between the latent variable  $E(\mathbf{x})$  and the underlying factor  $\boldsymbol{\xi}$  in the model.

### 5.1. DCVAE

We now proceed to present the full probabilistic formulation of DCVAE. The model's structure is depicted in Figure 1. The conditional generative model is defined as follows:

$$p_{\boldsymbol{\theta}}(\mathbf{x}, \tilde{\mathbf{z}}|\mathbf{u}) = p_{\mathbf{f}}(\mathbf{x}|\tilde{\mathbf{z}}, \mathbf{u})p_{\mathbf{T}, \boldsymbol{\lambda}}(\tilde{\mathbf{z}}|\mathbf{u}) \quad (8)$$

$$p_{\mathbf{f}}(\mathbf{x}|\tilde{\mathbf{z}}, \mathbf{u}) = p_{\mathbf{f}}(\mathbf{x}|\tilde{\mathbf{z}}) = p_{\boldsymbol{\zeta}}(\mathbf{x} - \mathbf{f}(\tilde{\mathbf{z}})) \quad (9)$$

$$p_{\mathbf{T}, \boldsymbol{\lambda}}(\tilde{\mathbf{z}}|\mathbf{u}) = \begin{cases} \frac{Q(\tilde{\mathbf{z}}_{< m})e^{\langle \mathbf{T}(\tilde{\mathbf{z}}_{< m}), \boldsymbol{\lambda}(\mathbf{u}) \rangle}}{Z(\mathbf{u})} \\ \mathcal{N}(\mathbf{0}_{(d-m) \times 1}, \mathbf{I}_{(d-m) \times (d-m)}) \end{cases} \quad (10)$$

where  $\boldsymbol{\theta} = (\mathbf{f}, \mathbf{T}, \boldsymbol{\lambda}) \in \boldsymbol{\Theta}$  are model parameters. Eq. (8) describes the process of generating  $\mathbf{x}$  from  $\tilde{\mathbf{z}}$ . Eq. (9) indicates that  $\mathbf{x} = \mathbf{f}(\tilde{\mathbf{z}}) + \boldsymbol{\zeta}$ , where  $p_{\boldsymbol{\zeta}}(\boldsymbol{\zeta}) = \mathcal{N}(\mathbf{0}, \mathbf{I})$  and the decoder  $\mathbf{f}(\tilde{\mathbf{z}})$  is assumed to be an invertible function, which is approximated by a neural network. As presented in Eq. (10), we use the exponential conditional distribution [49] for the first  $m$  dimensions and another distribution (e.g., standard normal distribution) for the remaining  $d-m$  dimensions to capture other non-interest factors for generation, where  $\mathbf{T} : \mathbb{R}^d \rightarrow \mathbb{R}^{d \times l}$  is the sufficient statistic,  $\boldsymbol{\lambda} : \mathbb{R}^k \rightarrow \mathbb{R}^{d \times l}$  is the corresponding parameter,  $Q : \mathbb{R}^d \rightarrow \mathbb{R}$  is the base measure,  $Z(\mathbf{u})$  is the normalizing constant and  $\langle \cdot, \cdot \rangle$  denotes the dot product. If  $d = m$ , we will only use the conditional prior in the first line of (10). When causal relationships exist among the generative factors of data  $\mathbf{x}$ , indicating their non-mutual independence, incorporating information  $\mathbf{u}$  alters the prior distribution from a factorial distribution to a distribution that better matches the real-world situation.

We define the inference model that utilizes causal flows as follows:

$$q_{\phi}(\mathbf{z}|\mathbf{x}, \mathbf{u}) = q_{\epsilon}(\mathbf{z} - \phi(\mathbf{x}, \mathbf{u})) \quad (11)$$

$$\mathbf{z} \sim q_{\phi}(\mathbf{z}|\mathbf{x}, \mathbf{u}) \quad (12)$$

$$\tilde{\mathbf{z}} = \mathbf{g}(\mathbf{z}, \mathbf{x}) \quad (13)$$

$$q_{\phi, \boldsymbol{\gamma}}(\tilde{\mathbf{z}}|\mathbf{x}, \mathbf{u}) = q_{\phi}(\mathbf{z}|\mathbf{x}, \mathbf{u}) \prod_{i=1}^d \exp(-s_i(\tilde{\mathbf{z}} \circ A_{i, \cdot}, \mathbf{x})) \quad (14)$$

where  $\boldsymbol{\gamma} = (\mathbf{s}, \mathbf{t}, A) \in \boldsymbol{\Gamma}$  denotes parameters of causal flows. Eq. (11) indicates that  $\mathbf{z} = \phi(\mathbf{x}, \mathbf{u}) + \epsilon$ , where the probability density of  $\epsilon$  is  $q_{\epsilon}(\epsilon) = \mathcal{N}(\mathbf{0}, \mathbf{I})$  and  $\phi(\mathbf{x}, \mathbf{u})$  denotes the encoder. Eq. (12) and (13) describe the process of transforming the original encoder output  $\mathbf{z}$  into the final latent variable representation  $\tilde{\mathbf{z}}$  by using causal flows. Eventually, the posterior distribution obtained by the inference model is represented by Eq. (14). So the parameters of stochastic transformation  $E(\mathbf{x}, \mathbf{u})$  are  $\phi$  and  $\boldsymbol{\gamma}$ .

Now the dataset  $\mathcal{X}$  has an empirical data distribution denoted by  $q_{\mathcal{X}}(\mathbf{x}, \mathbf{u})$ . Our goal is to maximize the variational

lower bound on the marginal likelihood  $p_{\theta}(\mathbf{x}|\mathbf{u})$ . The labels  $\mathbf{y}$  represent the ground-truth latent factors. We introduce a regularization term in the objective function to encourage consistency between  $\xi$  and  $E(\mathbf{x}, \mathbf{u})$ . The loss function of DCVAE is formulated as follows:

$$\begin{aligned} \mathcal{L}(\phi, \gamma, \theta) &= -\text{ELBO}(\phi, \gamma, \theta) + \beta_{sup} \mathcal{L}_{sup}(\phi, \gamma) \\ &= -\mathbb{E}_{q_{\mathbf{x}}} [\mathbb{E}_{q_{\phi, \gamma}(\tilde{\mathbf{z}}|\mathbf{x}, \mathbf{u})} \log p_{\mathbf{f}}(\mathbf{x}|\tilde{\mathbf{z}}, \mathbf{u}) \\ &\quad - D_{\text{KL}}(q_{\phi, \gamma}(\tilde{\mathbf{z}}|\mathbf{x}, \mathbf{u}) \| p_{\mathbf{T}, \lambda}(\tilde{\mathbf{z}}|\mathbf{u}))] \\ &\quad + \beta_{sup} \mathbb{E}_{(\mathbf{x}, \mathbf{y}, \mathbf{u})} [l_{sup}(\phi, \gamma)] \end{aligned} \quad (15)$$

where  $\beta_{sup} > 0$  is a hyperparameter,  $l_{sup}(\phi, \gamma) = \sum_{i=1}^m (\mathbf{y}_i - \bar{E}(\mathbf{x}, \mathbf{u})_i)^2$  is the Mean Squared Error (MSE) if  $\mathbf{y}_i$  is the continuous observation, and  $l_{sup}(\phi, \gamma) = \sum_{i=1}^m -\mathbf{y}_i \log \sigma(\bar{E}(\mathbf{x}, \mathbf{u})_i) - (1 - \mathbf{y}_i) \log (1 - \sigma(\bar{E}(\mathbf{x}, \mathbf{u})_i))$  is the cross-entropy loss if  $\mathbf{y}_i$  is the binary label. The loss term  $\mathcal{L}_{sup}$  aligns the factor of interest  $\xi \in \mathbb{R}^m$  with the first  $m$  dimensions of the latent variable  $\tilde{\mathbf{z}}$ , in order to satisfy the Definition 1 [24, 43].

## 5.2. Disentanglement Identifiability

We establish the identifiability of disentanglement of DCVAE, which confirms that our model can learn disentangled representations. We adopt the definition the model’s identifiability from [24]. As we only focus on disentangling the factors of interest, we will, for simplicity, present our theorem in the case where  $d = m$ . Here, we consider the deterministic part of the posterior distribution as the learned representation.

**Theorem 1** (Disentanglement Identifiability). *Under the assumptions of infinite capacity for  $E$  and  $\mathbf{f}$ , the solution  $(\phi^*, \gamma^*, \theta^*) \in \text{argmin}_{\phi, \gamma, \theta} \mathcal{L}(\phi, \gamma, \theta)$  of the loss function (15) guarantees that  $\bar{E}_{\phi^*, \gamma^*}(\mathbf{x})$  is disentangled with respect to  $\xi$ , as defined in Definition 1.*

*Proof.* See Appendix Appendix A.  $\square$

This theorem theoretically ensures that the learned representation, as defined by Definition 1, is a disentangled representation. Therefore, our model is capable of successfully learning disentangled representations even when there are causal relationships among latent factors.

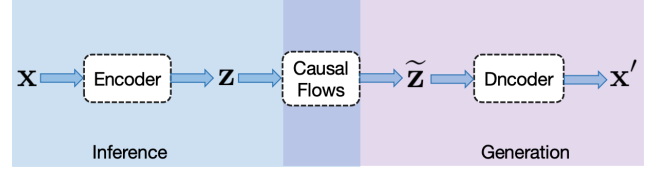


Figure 1: Model structure of DCVAE.

Shen et al. [24] demonstrated that even under the supervision of latent variables, the previously employed disentanglement representation learning methods based on the assumption of independent priors fail to achieve disentanglement when causal relationships exist among the latent factors of interest (i.e., the disentanglement identifiability mentioned earlier in our Definition 1). Therefore, to address the identifiability issue highlighted in Shen et al. [24], we incorporate additional information  $\mathbf{u}$  relevant to the true causal concepts as the supervision signal. In our work, we utilize concept labels as the additional information  $\mathbf{u}$  in two ways. Firstly, we propose utilizing conditional priors in VAE objective, to regularize the learned posterior of  $\mathbf{z}$ , enabling us to focus on priors of the generating factors of interest that are more aligned with reality. Secondly, the concept labels serve as regularization terms to regularize the latent variable information, i.e., as  $\mathbf{y}$ . Thus, the overall supervision signal used by the model consists solely of the labels of the generating factors. As mentioned in Section 2.2, the current methods predominantly focus on supervised models, which are implementable in practice, ensuring the applicability of our model. Exploring how to utilize our framework in semi-supervised or even unsupervised scenarios will be the focus of our future research.

## 6. Experiments

In this section, we empirically evaluate DCVAE, demonstrating that the learned representation is causally disentangled. This capability will enable the model to effectively perform across various tasks.

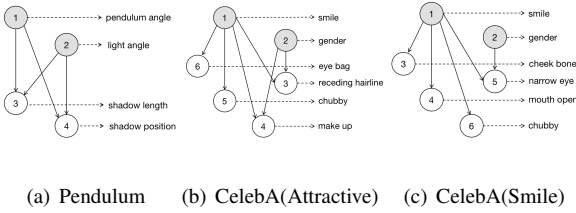


Figure 2: Causal graphs of Pendulum and CelebA. The gray circles represent the causal variables in the graphs. In Figures (a), (b), and (c), we label the underlying factors we are interested in each dataset.

### 6.1. Datasets

We utilize the same datasets from Shen et al. [24] where the underlying generative factors are causally related. The synthetic dataset is Pendulum, with four continuous factors whose causal graph of the factors is shown in Figure 2(a). We generate the pendulum dataset using the synthetic simulators mentioned in Yang et al. [25]. The training and testing sets consist of 5847 and 1461 samples, respectively. The real human face dataset is CelebA [50], with 40 discrete labels. We consider two sets of causally related factors named CelebA(Attractive) and CelebA(Smile) with causal graphs also depicted in Figure 2(b) and 2(c). We set the values of features that are  $-1$  to  $0$ . The training and testing sets consist of 162770 and 19962 samples, respectively. All the images are resized to  $64 \times 64 \times 3$  resolution.

### 6.2. Experimental Settings and Baselines

We present the main settings used in our experiments. Our experiments on Pendulum utilize one NVIDIA GeForce RTX 2080ti GPU, while experiments on CelebA use one NVIDIA GeForce RTX 3080 GPU. To train DEAR, we use two NVIDIA GeForce RTX 2080ti GPUs.

#### 6.2.1. DCVAE

In DCVAE, regarding the setting of conditional prior of DCVAE, since it is generally difficult to directly fit the exponential family of distributions, we use a special form of exponential distribution, namely the Gaussian distribution in our experiments. For simplicity, we adopt a factorial distribution, as described in Khemakhem et al. [44] and Yang et al. [25]. However, unlike

them, we set the *mean* and *variance* as learnable parameters for training, which enhances the flexibility of the prior distribution. In the implementation of the supervised loss for Pendulum, the factors’ labels are resized to  $[-1, 1]$  because they are continuous, and Mean Squared Error (MSE) is employed as the loss function  $\mathcal{L}_{sup}$ . For CelebA, where the factors’ labels are binary, we map  $-1$  to  $0$  and utilize cross-entropy loss. The comprehensive details of the network architectures and hyperparameters are given in Appendix Appendix B.

#### 6.2.2. Baseline models

We compare our method with several state-of-the-art VAE-based models for disentanglement [2], including  $\beta$ -VAE [16],  $\beta$ -TCVAE [19], DEAR [24] and VAE [11]. We also investigate prior information with limited understanding of causal graph structures. Specifically, DCVAE-SP represents a DCVAE trained using the given super-graph of the true graph (i.e., Figure 7), rather than the full graph. In this context,  $\beta$ -VAE and  $\beta$ -TCVAE stand out as the most representative VAE-based disentanglement models, imposing independent constraints on the posterior and utilizing total correlation to encourage independence among aggregated posteriors, respectively. Currently, the most advanced causal disentanglement model based on VAE is DEAR. Therefore, overall, the selected comparison models are all representative. We use the same conditional prior and loss term with labeled data for each of these methods as in DCVAE, except that DEAR’s prior is SCM prior. Furthermore, apart from models that specifically choose the architecture of encoder and decoder, we employ identical encoder and decoder structures for the baselines. The implementations of  $\beta$ -TCVAE and DEAR are each associated with publicly available source codes, which can be found at <https://github.com/AntixK/PyTorch-VAE> and <http://jmlr.org/papers/v23/21-0080.html>.

It is worth noting that we did not compare our results with the model in Yang et al. [25]. Firstly, due to the presence of a Mask layer in its decoder, it is not possible to observe changes in individual factors when traversing each dimension of the learned

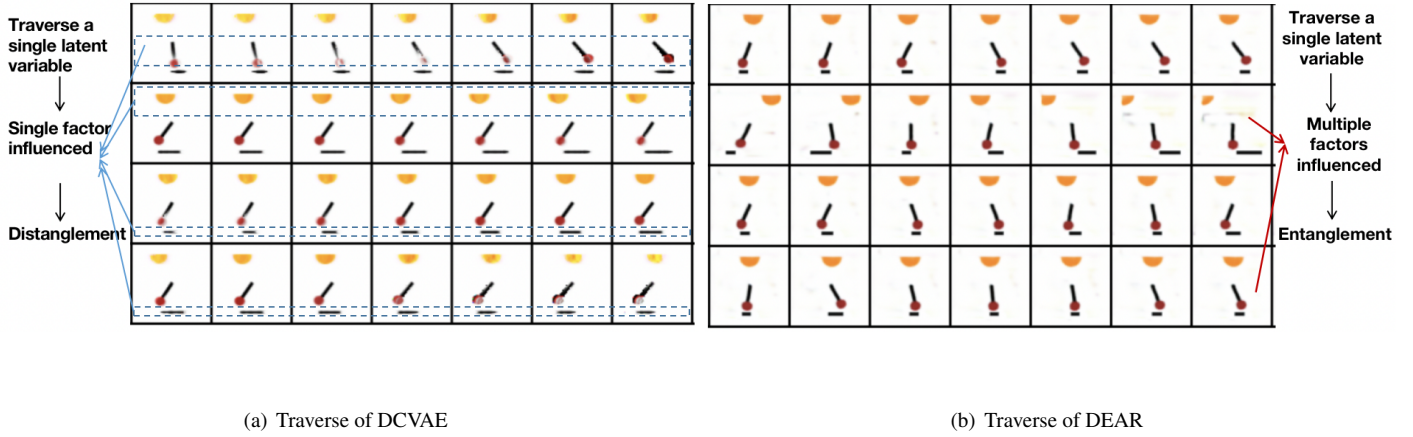


Figure 3: Results of traverse experiments on Pendulum. Each row corresponds to a variable that we traverse on, specifically, pendulum angle, light angle, shadow length, and shadow position.

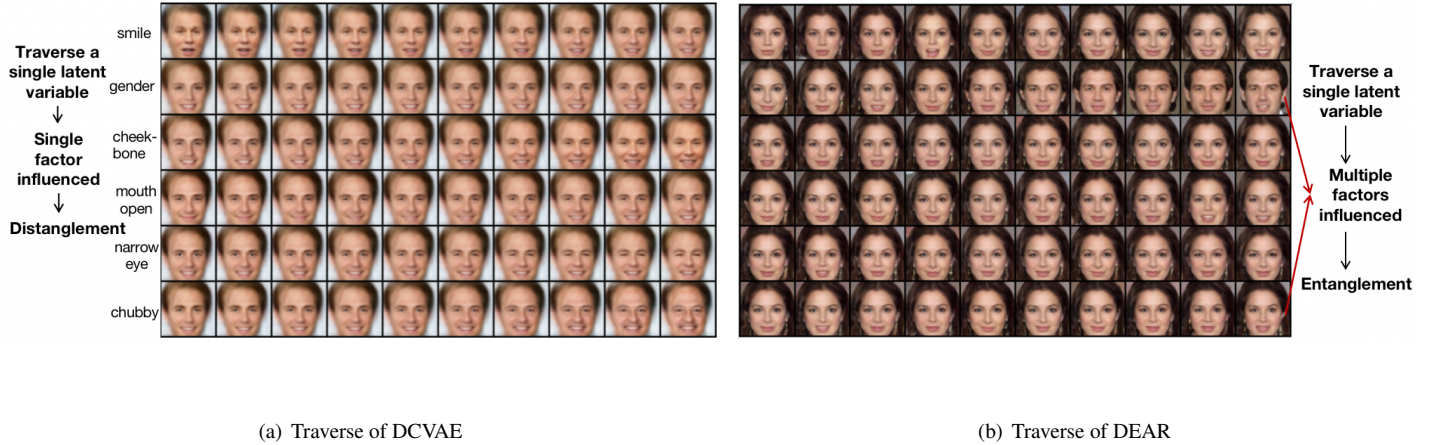


Figure 4: Results of traverse experiments on CelebA(Smile). Each row corresponds to a variable that we traverse on, specifically, smile, gender, cheek bone, mouth open, narrow eye and chubby.

representation. Secondly, the latent variable dimension in the model corresponds to the number of interested latent factors, which, when applied to real-world datasets, may not enable the latent layer to capture all the generative factors of the images, thereby failing to ensure a one-to-one correspondence between latent units and generative factors, and consequently, not achieving causal disentanglement. In comparison, DEAR, as a VAE-based causal disentanglement model, is more reasonable. To ensure a fair comparison with equal amounts of supervised information, for each of these methods we use the same conditional prior and loss term as in DCVAE.

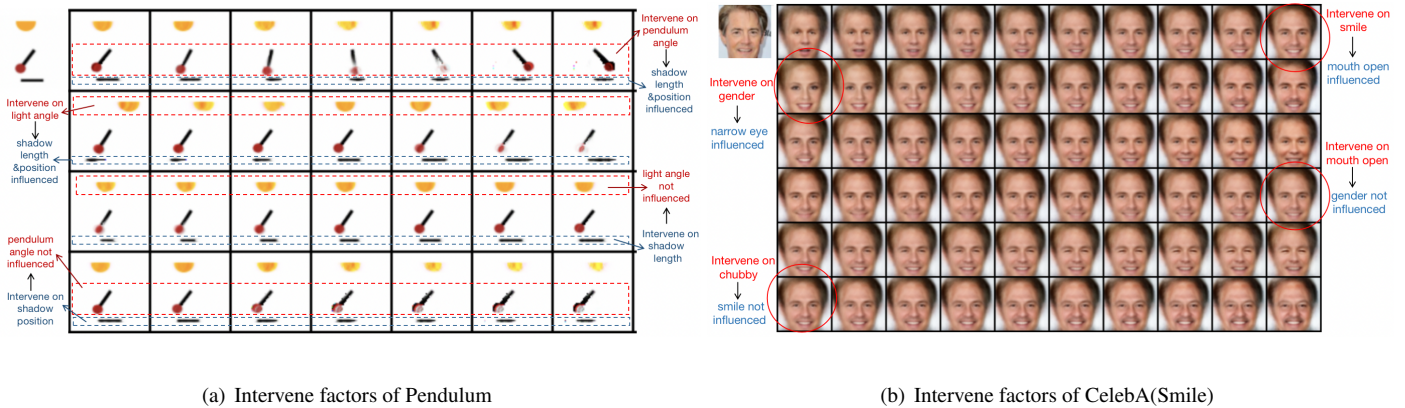
### 6.3. Experimental Results

Now, we proceed to evaluate our method through both qualitative and quantitative experiments and provide an analysis of the corresponding experimental results.

#### 6.3.1. Causal Disentangled Representations

To qualitatively verify that DCVAE indeed learns causal disentangled representations, we conduct intervention experiments.

Intervention experiments involve performing the "do-operation" in causal inference [51]. Taking a single-step causal flow as an example, we demonstrate step by step how our model performs "do-operation". First, given a trained model, we input the sample



(a) Intervene factors of Pendulum

(b) Intervene factors of CelebA(Smile)

Figure 5: Results of intervention on only one variable for both Pendulum and CelebA(Smile). The image in the upper left corner of (a) and (b) are the test data we consider respectively.

$\mathbf{x}$  into the inference model, obtaining an output  $\tilde{\mathbf{z}}$ . Assuming we wish to perform the "do-operation" on  $\tilde{\mathbf{z}}_i$ , i.e.,  $do(\tilde{\mathbf{z}}_i = c)$ , we follow the approach in Khemakhem et al. [37] by treating Eq. (4) as SEMs. Specifically, we set the input and output of  $\tilde{\mathbf{z}}_i$  to the control value  $c$ , while other values are computed iteratively from input to output. Finally, the resulting  $\tilde{\mathbf{z}}$  is decoded to generate the desired image, which corresponds to generating images from the interventional distribution of  $\tilde{\mathbf{z}}$ .

We perform intervention experiments by applying the "do-operation" to  $m - 1$  variables in the first  $m$  dimensions of the latent variables, resulting in the change of only one variable. This operation, which has been referred to as "traverse", aims to test the disentanglement of our model [24]. Figures 3 and 4 show the experimental results of the DCVAE and DEAR on Pendulum and CelebA(Smile). We observe that when traversing a latent variable dimension, DCVAE has almost only one factor changing, while DEAR has multiple factors changing. This is clearly shown by comparing "traverse" results of the third row for shadow length in Figures 3(a) and 3(b), as well as the second row for gender in Figures 4(a) and 4(b). Therefore, our model performs better in achieving causal disentanglement.

To demonstrate our model's capability to perform interventions hence generating new images beyond the dataset, we further conduct "do-operations" on individual latent variables. Figure 5 illustrates these operations, with each row representing an

intervention on a single dimension. In Figure 5(a), we observe that intervening on the pendulum angle and light angle produces changes in shadow length in accordance with physical principles. However, intervening on shadow length has minimal impact on these two factors. Similarly, as illustrated in Figure 5(b), intervening on gender influences narrow eye appearance, but the reverse is not true. This demonstrates that intervening on causal factors affects the resulting effects, but not the other way around. Hence, our latent variables have effectively learned factor representations, attributed to the design of the causal flows, which incorporate  $A$ . Additional traversal and intervention results are presented in Appendix Appendix C.

### 6.3.2. Downstream tasks

To quantitatively illustrate benefits of causal disentangled representations, we consider its impact on downstream tasks in terms of sample efficiency and distributional robustness. We introduce two downstream prediction tasks to compare our model with baseline models. First, for Pendulum, we normalize factors to  $[-1, 1]$  during preprocessing. Then, we manually create a classification task: if  $pendulum\ angle > 0$  and  $light\ angle > 0$ , the target label  $y = 1$ ; otherwise,  $y = 0$ . For the CelebA(Attractive), we adopt the same classification task as presented in [24]. We employ multilayer perceptron (MLP) to train classification models, where both the training and testing sets consist of the latent representations  $\tilde{\mathbf{z}}$  and their

Table 1: Test accuracy and sample efficiency of different models on Pendulum and CelebA datasets. Mean $\pm$ standard deviations are included in the Table.

Model	Pendulum			CelebA		
	100(%)	All(%)	Sample Eff	100(%)	10000(%)	Sample Eff
DCVAE	<b>99.00<math>\pm</math>0</b>	99.43 $\pm$ 0.34	<b>99.57<math>\pm</math>0.34</b>	<b>81.00<math>\pm</math>1.73</b>	<b>81.54<math>\pm</math>1.76</b>	<b>99.34<math>\pm</math>0.27</b>
DCVAE-SP	98.67 $\pm$ 0.58	<b>99.79<math>\pm</math>0.14</b>	98.87 $\pm$ 0.70	79.67 $\pm$ 1.15	81.32 $\pm$ 0.47	97.98 $\pm$ 1.69
DEAR	88.00 $\pm$ 0	88.55 $\pm$ 0.04	98.63 $\pm$ 1.33	61.00 $\pm$ 3.60	68.50 $\pm$ 0	89.05 $\pm$ 5.26
$\beta$ -VAE	98.67 $\pm$ 1.15	99.59 $\pm$ 0.07	98.94 $\pm$ 0.92	62.33 $\pm$ 5.69	68.49 $\pm$ 0.02	91.01 $\pm$ 8.28
$\beta$ -TCVAE	97.67 $\pm$ 1.15	99.38 $\pm$ 0.48	98.27 $\pm$ 0.79	75.33 $\pm$ 3.21	78.72 $\pm$ 4.93	95.83 $\pm$ 4.10
VAE	98.33 $\pm$ 0.58	99.48 $\pm$ 0.39	98.72 $\pm$ 0.37	60.33 $\pm$ 2.89	68.50 $\pm$ 0	88.08 $\pm$ 4.21

Table 2: Distributional robustness of different models.

Model	TestAvg(%)	TestWorst(%)
DCVAE	<b>97.83<math>\pm</math>1.18</b>	<b>94.70<math>\pm</math>3.41</b>
DCVAE-SP	97.24 $\pm$ 0.49	92.43 $\pm$ 0.54
DEAR	80.40 $\pm$ 0.47	64.50 $\pm$ 2.67
$\beta$ -VAE	96.48 $\pm$ 2.06	90.05 $\pm$ 5.44
$\beta$ -TCVAE	96.57 $\pm$ 1.33	90.27 $\pm$ 3.74
VAE	95.14 $\pm$ 3.46	88.81 $\pm$ 5.44

corresponding labels  $y$ .

**Sample Efficiency:** The experimental results are presented in Table 1. We adopt the statistical efficiency score defined in Locatello et al. [2] as a measure of sample efficiency, which is defined as the classification accuracy of 100 test samples divided by the number of all (Pendulum)/10,000 test samples (CelebA). Table 1 shows that DCVAE achieves the best sample efficiency on both datasets. DCVAE-SP exhibits slightly inferior performance compared to DCVAE, but it remains competitive when compared to other baseline methods. Hence, while the model’s optimal performance is achieved by integrating information from the full graph, causal flows can still contribute with slightly diminished effectiveness in the case of the super-graph. This emphasizes the significance of incorporating causal flow in our model. We attribute the superiority of DCVAE to our modeling approach, which leverages the capabilities of causal flows and incorporates conditional prior. This greatly enhances the encoder’s ability to learn semantically meaningful and expressive

representations.

**Distributional robustness:** To assess distributional robustness, we modify the controllable synthetic Pendulum dataset during training to inject spurious correlations between the target label and some spurious attributes. We choose *background\_color*  $\in \{blue(+), white(-)\}$  as a spurious feature. Specifically, in 80% of the examples, the target label and the spurious attribute are both positive or negative, while in 20% of the examples, they are opposite. For instance, in the manipulated training set, 80% positive examples in Pendulum are masked with a blue background. But in the test set, we do not inject this correlation, resulting in a distribution shift. The results are summarized in Table 2.

The results include average and worst-case test accuracy, evaluating overall classification performance and distributional robustness. Worst-case accuracy identifies the group with the lowest accuracy among four groups categorized based on target and spurious binary labels. It often involves opposing spurious correlations compared to training data. The classifiers trained using DCVAE representations demonstrate significant superiority over all baseline models in both evaluation metrics. Notably, DCVAE experiences a smaller decrease in worst-case accuracy compared to average accuracy, indicating robustness to distributional shifts.

### 6.3.3. Exploring the potential for learning the structure $A$

Apart from the aforementioned applications, DCVAE has the potential to learn true causal relationships between factors, despite the fact that it is not the primary focus of our work. As

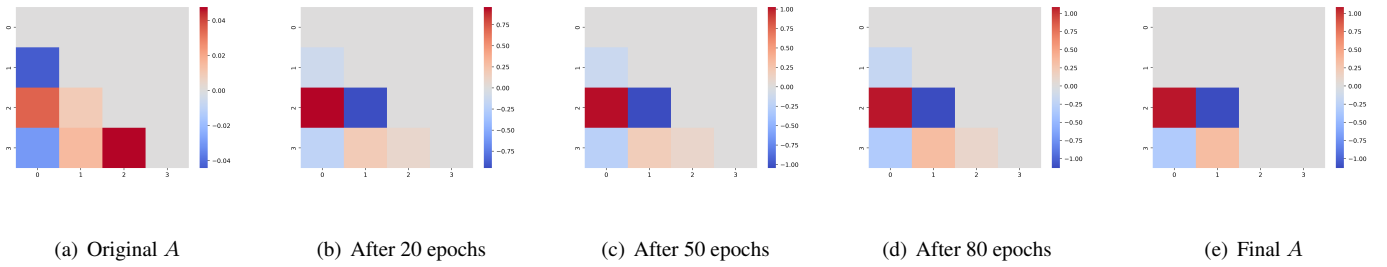


Figure 6: The learned weighted adjacency matrix  $A$  given the causal ordering on Pendulum. (a)-(d) illustrate the changes in  $A$  as the training progresses. (e) represents  $A$  after edge pruning.

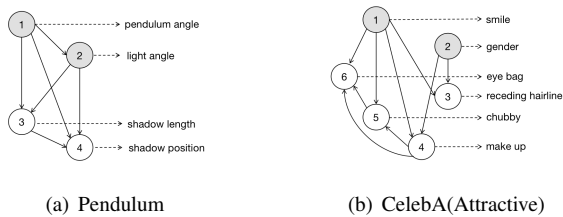


Figure 7: Super-graph of Pendulum and CelebA(Attractive).

shown in Figure 6(a)-6(d), for Pendulum, when our model  $A$  adopts the full graph shown in Figure 7(a), though the corresponding  $A$  is initialized randomly around 0, it gradually approaches the true causal structure during the training process. If we apply a threshold and prune edges in the causal graph, we obtain Figure 6(e), which corresponds to the true causal structure depicted in Figure 2(a). At this point, only four positions in matrix  $A$  are relatively large non-zero values, indicating accurate causal relationships. For the experiments conducted on CelebA dataset, please refer to Appendix Appendix C. This preliminary result suggests that our model has the potential to learn causal structures even without relying on a Structural Causal Model (SCM) [25, 52], inspiring us to explore this topic further in future research.

## 7. Conclusion and Points of Future Research

In this paper, we focus on addressing the significant challenge of learning causal disentangled representations using VAE when the underlying generative factors are causally related. We propose the Disentangled Causal Variational Auto-Encoder (DCVAE), which leverages causal flows to integrate the causal struc-

ture information of generative factors into the model. Through rigorous theoretical analysis, we demonstrate that DCVAE achieves disentanglement identifiability by incorporating supervised information. Empirical results, including quantitative and qualitative experiments on synthetic and real-world datasets, validate our method’s success in learning causal disentangled representations and generating counterfactual outputs.

For future research directions, there are several aspects to consider. Firstly, our model focuses on a relatively small number of generative factors of interest. There is an opportunity to extend this to model causal relationships among a larger set of generative factors, which is particularly relevant in the era of big data. Currently, we have provided only a framework-inspired approach in this regard. Secondly, our model utilizes label information of generative factors. Future research could explore alternative forms of supervised information and further investigate semi-supervised or even unsupervised learning methods for causal disentangled representations within the framework of flow models. Lastly, delving deeper into exploring and leveraging the inherent structure of data itself to effectively learn low-dimensional causal disentangled representations presents a promising avenue for exploration. Furthermore, applying these causal disentangled representations to areas such as video generation is also a promising research direction.

## Appendix A. Proof of Theorem 1

We first present the properties of the exponential family distribution. Then we provide the proof of theorem 1.

**Definition 2 (Exponential family).** A probability distribution belongs to the exponential family if its density has the following form:

$$p(\mathbf{x}|\boldsymbol{\theta}) = \frac{Q(\mathbf{x})e^{\langle \mathbf{T}(\mathbf{x}), \boldsymbol{\lambda}(\boldsymbol{\theta}) \rangle}}{Z(\boldsymbol{\theta})} \quad (\text{A.1})$$

where  $\mathbf{x} \in \mathcal{X}$  and  $\boldsymbol{\theta} \in \Theta$ ,  $\mathbf{T} : \mathcal{X} \rightarrow \mathbb{R}^k$  is the sufficient statistic,  $\boldsymbol{\lambda} : \Theta \rightarrow \mathbb{R}^k$  is the corresponding parameter,  $Q : \mathcal{X} \rightarrow \mathbb{R}$  is the base measure (Lebesgue measure),  $Z(\boldsymbol{\theta})$  is the normalizing constant and  $\langle \cdot, \cdot \rangle$  stands for the dot product. More precisely, we can refer to Eq. (A.1) as conditional exponential family [49].

**Theorem 1** (Khemakhem et al. [53]). *Let  $p(\mathbf{x}|\boldsymbol{\theta})$  be a conditional probability density function. Assume that  $\mathcal{X}$  and  $\Theta$  are compact Hausdorff spaces, and that  $p(\mathbf{x}|\boldsymbol{\theta}) > 0$  almost surely  $\forall (\mathbf{x}, \boldsymbol{\theta}) \in \mathcal{X} \times \Theta$ . Then for each  $\epsilon > 0$ , there exists  $(\phi, k) \in \Phi \times \mathbb{N}$ ,  $\phi = (\mathbf{T}, \boldsymbol{\lambda})$ , where  $k$  is the dimension of the feature extractor, such that  $\sup_{(\mathbf{x}, \boldsymbol{\theta}) \in \mathcal{X} \times \Theta} |p_{\boldsymbol{\theta}}(\mathbf{x}|\boldsymbol{\theta}) - p(\mathbf{x}|\boldsymbol{\theta})| < \epsilon$ .*

The above theorem shows the universal approximation capability of conditional exponential family. Specifically, they showed that for compact Hausdorff spaces  $\mathcal{X}$  and  $\Theta$ , any conditional probability density  $p(\mathbf{x}|\boldsymbol{\theta})$  can be approximated arbitrarily well. Thus, through the consideration of a freely varying  $k$ , and general  $\mathbf{T}$  and  $\boldsymbol{\lambda}$ , the conditional exponential family is endowed with universal approximation capability over the set of conditional probability densities. In practice, it is possible to achieve almost perfect approximation by choosing  $k$  greater than the input dimension. However, this result does not take into account the practicality of fitting the approximation family to data, and increasing  $k$  may make it more difficult to fit the data distribution in real-world scenarios.

We now prove Theorem 1.

*Proof.* Following the approach in [24], we give a proof of this theorem. We suppose that  $d = m$ . For  $\forall i = 1, 2, \dots, m$ , we consider two cases separately. In the first case,  $\mathcal{L}_{sup,i}(\phi, \gamma)$  is cross-entropy loss:

$$\begin{aligned} \mathcal{L}_{sup,i}(\phi, \gamma) &= \mathbb{E}_{(\mathbf{x}, \mathbf{y}, \mathbf{u})} [-\mathbf{y}_i \log \sigma(\bar{E}(\mathbf{x}, \mathbf{u})_i) \\ &\quad - (1 - \mathbf{y}_i) \log (1 - \sigma(\bar{E}(\mathbf{x}, \mathbf{u})_i))] \\ &= - \int q(\mathbf{x}, \mathbf{u}) p(\mathbf{y}_i | \mathbf{x}, \mathbf{u}) [\mathbf{y}_i \log \sigma(\bar{E}(\mathbf{x}, \mathbf{u})_i) \end{aligned}$$

$$+ (1 - \mathbf{y}_i) \log (1 - \sigma(\bar{E}(\mathbf{x}, \mathbf{u})_i))] dx d\mathbf{u} d\mathbf{y}_i \quad (\text{A.2})$$

where  $P(\mathbf{y}_i = 1 | \mathbf{x}, \mathbf{u}) = \mathbb{E}(\mathbf{y}_i | \mathbf{x}, \mathbf{u})$ ,  $P(\mathbf{y}_i = 0 | \mathbf{x}, \mathbf{u}) = 1 - \mathbb{E}(\mathbf{y}_i | \mathbf{x}, \mathbf{u})$ . Let  $\frac{\partial \mathcal{L}_{sup,i}(\phi, \gamma)}{\partial \sigma(\bar{E}(\mathbf{x}, \mathbf{u})_i)} = 0$ , we know that  $\bar{E}^*(\mathbf{x}, \mathbf{u})_i = \sigma^{-1}(\mathbb{E}(\mathbf{y}_i | \mathbf{x}, \mathbf{u})) = \sigma^{-1}(\xi_i)$  can minimize  $\mathcal{L}_{sup,i}(\phi, \gamma)$ .

In the second case,  $\mathcal{L}_{sup,i}(\phi, \gamma)$  is Mean Squared Error (MSE):

$$\begin{aligned} \mathcal{L}_{sup,i}(\phi, \gamma) &= \mathbb{E}_{(\mathbf{x}, \mathbf{y}, \mathbf{u})} [(\mathbf{y}_i - \bar{E}(\mathbf{x}, \mathbf{u})_i)^2] \\ &= \int q(\mathbf{x}, \mathbf{u}) p(\mathbf{y}_i | \mathbf{x}, \mathbf{u}) (\mathbf{y}_i - \bar{E}(\mathbf{x}, \mathbf{u})_i)^2 dx d\mathbf{u} d\mathbf{y}_i \end{aligned} \quad (\text{A.3})$$

Let  $\frac{\partial \mathcal{L}_{sup,i}(\phi, \gamma)}{\partial \sigma(\bar{E}(\mathbf{x}, \mathbf{u})_i)} = 0$ , we know that  $\bar{E}^*(\mathbf{x}, \mathbf{u})_i = \mathbb{E}(\mathbf{y}_i | \mathbf{x}, \mathbf{u}) = \xi_i$  can minimize the  $\mathcal{L}_{sup,i}(\phi, \gamma)$ .

Next, because of the infinite capacity of  $\mathbf{f}$  and Theorem 2, we know that  $q_{\phi^*, \gamma^*}(\mathbf{x}, \tilde{\mathbf{z}} | \mathbf{u})$  is contained within the distribution family of  $p_{\boldsymbol{\theta}}(\mathbf{x}, \tilde{\mathbf{z}} | \mathbf{u})$ . Then by minimizing the loss in (15) over  $\boldsymbol{\theta}$ , we can find  $\boldsymbol{\theta}^*$  such that  $p_{\boldsymbol{\theta}^*}(\mathbf{x}, \tilde{\mathbf{z}} | \mathbf{u})$  matches  $q_{\phi^*, \gamma^*}(\mathbf{x}, \tilde{\mathbf{z}} | \mathbf{u})$  and thus

$$\begin{aligned} -\text{ELBO}(\phi^*, \gamma^*, \boldsymbol{\theta}^*) &= D_{\text{KL}}(q_{\phi^*, \gamma^*}(\mathbf{x}, \tilde{\mathbf{z}} | \mathbf{u}) \| p_{\boldsymbol{\theta}^*}(\mathbf{x}, \tilde{\mathbf{z}} | \mathbf{u})) \\ &\quad + \text{constant} \end{aligned} \quad (\text{A.4})$$

reaches minimum.

Therefore, by minimizing the loss function (15) of DC-VAE, we can get the solution, that is,  $\bar{E}^*(\mathbf{x}, \mathbf{u})_i = r_i(\xi_i)$  with  $r_i(\xi_i) = \sigma^{-1}(\xi_i)$  if cross-entropy loss is used, and  $r_i(\xi_i) = \xi_i$  if MSE is used. Here,  $\mathbf{x}$  denotes random variable.

To sum up,  $\bar{E}_{\phi^*, \gamma^*}(\mathbf{x}, \mathbf{u})$  is disentangled with respect to  $\boldsymbol{\xi}$ , as defined in Definition 1.  $\square$

## Appendix B. Experimental Details

We present the network architecture and hyperparameters used in our experiments. The network structures of encoder and decoder are presented in Table B.1. The encoder's output, i.e., *mean* and *log variance*, share parameters except for the final layer. A single-layer causal flow implemented by an MLP implementation is used for fitting the posterior distribution, and

Table B.1: Architecture for the Encoder and Decoder in DCVAE ( $d = 4$  for Pendulum and  $d = 100$  for CelebA).

Encoder	Decoder
-	Input $\tilde{\mathbf{z}} \in \mathbb{R}^d$
$3 \times 3$ conv, MaxPool, 8 SELU, stride 1	FC, 256 SELU
$3 \times 3$ conv, MaxPool, 16 SELU, stride 1	FC, $16 \times 12 \times 12$ SELU
$3 \times 3$ conv, MaxPool, 32 SELU, stride 1	$2 \times 2$ conv, 32 SELU, stride 1
$3 \times 3$ conv, MaxPool, 64 SELU, stride 1	$2 \times 2$ conv, 64 SELU, stride 1
$3 \times 3$ conv, MaxPool, 8 SELU, stride 1	$2 \times 2$ conv, 128 SELU, stride 1
FC $256 \times 2$	FC, $3 \times 64 \times 64$ Tanh

Table B.2: Hyperparameters of DCVAE.

Parameters	Values (Pendulum)	Values (CelebA)
Batch size	128	128
Epoch	801	101
Latent dimension	4	100
$\sigma$	0.1667	0.1667
$\beta_{sup}$	8	5
$\beta_1$	0.2	0.2
$\beta_2$	0.999	0.999
$\epsilon$	$1e-8$	$1e-8$
Learning rate of Encoder	$5e-5$	$3e-4$
Learning rate of Causal Flow	$5e-5$	$3e-4$
Learning rate of $A$	$1e-3$	$1e-3$
Learning rate of Conditional prior	$5e-5$	$3e-4$
Learning rate of Decoder	$5e-5$	$3e-4$

a causal weight matrix  $A$  is added in a manner inspired by Wehenkel and Louppe [38]. The decoder’s output is resized to generate pixel values for a three-channel color image. We train the model using the Adam optimizer, and all the training parameters are shown in Table B.2. Although we cannot guarantee finding the optimal solution in the experiments, the empirical results still demonstrate the excellent performance of our model.

## Appendix C. Additional Results

### Appendix C.1. Samples from interventional distributions

In section 6.3.1, we describe the capability of our model to perform interventions by generating new images that do not exist in the dataset. Specifically, our model utilizes causal flows to sample from the interventional distributions, even though the

model is trained on observational data. The steps for intervening on one factor are explained in section 6.3.1, and the same applies to intervening on multiple factors. As depicted in Figure 1(a), we intervene on the values of two factors by fixing gender as female and gradually adjusting the value of receding hairline. This produces a series of images showing women with a gradually receding hairline. Furthermore, as shown in Figure 1(b), we intervene on gender and makeup, generating a series of images of men with gradually applied makeup. These images are not commonly found or may not even exist in the training data, highlighting the ability of our model to sample from interventional distributions.

### Appendix C.2. Learning of causal structure

DCVAE has the potential to learn causal structure between underlying factors, even though our work does not specifically focus on this aspect, and it does not use the Structural Causal Model (SCM) framework. Here we present the learning process of the adjacency weight matrix  $A$ , whose super-graph is shown in Figure 7. Figure C.3 shows the learning process of CelebA (Attractive). If we set a threshold of 0.25, i.e., considering edges in the causal graph smaller than the threshold as non-existing, we can obtain Figure 3(e). Our observation indicates that DCVAE effectively eliminates a significant portion of redundant variables and ultimately achieves a nearly accurate graph. This suggests the potential for further improvements in causal discovery through future research work.

### Appendix C.3. Examining Causal Disentangled Representations

To verify whether our model has learned causal disentangled representations, we consider two types of intervention operations: the "traverse" operation and the "intervention" operation introduced in Section 6.3.1. We present the experimental results of DCVAE on CelebA(Attractive) in Figure C.4 and the results of baseline models on three datasets in Figure C.5, C.6, and C.7.

## Appendix D. Reflections on Disentanglement Metrics

Numerous disentanglement studies introduce their own metrics for assessing disentanglement, including the  $\beta$ -VAE metric [16], the FactorVAE metric [18], the Mutual Information Gap (MIG) [19], DCI [54] and more. For a comprehensive overview and discussion of these metrics, we direct readers to Locatello et al. [2]. However, all these metrics are applicable only in scenarios where the underlying generative factors are mutually independent; they do not extend to cases where factors exhibit correlation. As an illustration [24], the MIG score gauges the normalized gap in mutual information for each factor between the highest and second highest coordinates in  $\bar{E}(\mathbf{x}, \mathbf{u})$ . Consider a situation where factor  $\xi_1$  is correlated with  $\xi_2$ , and a disentangled representation  $\bar{E}(\mathbf{x}, \mathbf{u})$  is such that it accommodates one-to-one functions,  $r_1$  and  $r_2$ , leading to  $\bar{E}_1(\mathbf{x}, \mathbf{u}) = r_1(\xi_1)$

and  $\bar{E}_2(\mathbf{x}, \mathbf{u}) = r_2(\xi_2)$ . Consequently, both the mutual information of  $\xi_1$  with the highest coordinate  $\bar{E}_1(\mathbf{x}, \mathbf{u})$  and the second highest coordinate  $\bar{E}_2(\mathbf{x}, \mathbf{u})$  would be substantial, resulting in a minimal difference between them. As a consequence, a disentangled representation in this context would not yield the anticipated high MIG score. So far, the literature on metrics for causal disentanglement is limited and each has its shortcomings. Shen et al. [24] proposed a metric based on the FactorVAE metric. Compared to metrics like IRS [26] and (UC and GC) [27] that apply only under the assumption of conditional independence of generative factors, this metric is the only suitable one for our model. However, Kim et al. [21] showed this metric does not work well. The FactorVAE metric may only be partially indicative of the underlying disentanglement: all models attain a perfect scores, which is also confirmed in our experiments. The results revealed in our supplementary experiments show that the FactorVAE scores [24] obtained on DCVAE, VAE,  $\beta$ -TCVAE,  $\beta$ -VAE, and DEAR were 0.50, 0.50, 0.50, 0.50, and 0.28, respectively. Such outcomes indicate that, at the very least, our model is superior to the latest models DEAR in the causal disentangled representation learning. However, it is evident that there are shortcomings associated with this metric.

Hence, for quantitative assessment, we conduct experiments on downstream tasks to demonstrate the superiority of our model. Both in downstream tasks and qualitative studies, the outstanding performance of our model is evident.

## References

- [1] Y. Bengio, A. Courville, P. Vincent, Representation learning: A review and new perspectives, *IEEE transactions on pattern analysis and machine intelligence* 35 (2013) 1798–1828.
- [2] F. Locatello, S. Bauer, M. Lucic, G. Raetsch, S. Gelly, B. Schölkopf, O. Bachem, Challenging common assumptions in the unsupervised learning of disentangled representations, in: *International conference on machine learning*, PMLR, 2019, pp. 4114–4124.
- [3] J.-T. Hsieh, B. Liu, D.-A. Huang, L. F. Fei-Fei, J. C. Niebles, Learning to decompose and disentangle representations for video prediction, *Advances in neural information processing systems* 31 (2018).
- [4] J. Ma, C. Zhou, P. Cui, H. Yang, W. Zhu, Learning disentangled represen-

- tations for recommendation, *Advances in neural information processing systems* 32 (2019).
- [5] S. Mu, Y. Li, W. X. Zhao, S. Li, J.-R. Wen, Knowledge-guided disentangled representation learning for recommender systems, *ACM Transactions on Information Systems (TOIS)* 40 (2021) 1–26.
- [6] H. Zhang, R. K. Wong, V. W. Chu, Hybrid variational autoencoder for recommender systems, *ACM Transactions on Knowledge Discovery from Data (TKDD)* 16 (2021) 1–37.
- [7] S. Wang, X. Chen, Q. Z. Sheng, Y. Zhang, L. Yao, Causal disentangled variational auto-encoder for preference understanding in recommendation, *arXiv preprint arXiv:2304.07922* (2023).
- [8] D. Yang, S. Huang, H. Kuang, Y. Du, L. Zhang, Disentangled representation learning for multimodal emotion recognition, in: *Proceedings of the 30th ACM International Conference on Multimedia*, 2022, pp. 1642–1651.
- [9] X. Wang, H. Chen, W. Zhu, Disentangled representation learning for multimedia, in: *Proceedings of the 31st ACM International Conference on Multimedia*, 2023, pp. 9702–9704.
- [10] T. Jia, J. Li, L. Zhuo, J. Zhang, Self-guided disentangled representation learning for single image dehazing, *Neural Networks* 172 (2024) 106107.
- [11] D. P. Kingma, M. Welling, Auto-encoding variational bayes, *arXiv preprint arXiv:1312.6114* (2013).
- [12] M. A. Chao, B. T. Adey, O. Fink, Implicit supervision for fault detection and segmentation of emerging fault types with deep variational autoencoders, *Neurocomputing* 454 (2021) 324–338.
- [13] Q. Wang, T. P. Breckon, Generalized zero-shot domain adaptation via coupled conditional variational autoencoders, *Neural Networks* 163 (2023) 40–52.
- [14] A. Caciularu, J. Goldberger, An entangled mixture of variational autoencoders approach to deep clustering, *Neurocomputing* 529 (2023) 182–189.
- [15] S. Leglaive, A multimodal dynamical variational autoencoder for audiovisual speech representation learning, in: *Proceedings of the 1st International Workshop on Methodologies for Multimedia*, 2022, pp. 3–3.
- [16] I. Higgins, L. Matthey, A. Pal, C. Burgess, X. Glorot, M. Botvinick, S. Mohamed, A. Lerchner, beta-vae: Learning basic visual concepts with a constrained variational framework, in: *International conference on learning representations*, 2017.
- [17] C. P. Burgess, I. Higgins, A. Pal, L. Matthey, N. Watters, G. Desjardins, A. Lerchner, Understanding disentangling in  $\beta$ -vae, *arXiv preprint arXiv:1804.03599* (2018).
- [18] H. Kim, A. Mnih, Disentangling by factorising, in: *International Conference on Machine Learning*, PMLR, 2018, pp. 2649–2658.
- [19] R. T. Chen, X. Li, R. B. Grosse, D. K. Duvenaud, Isolating sources of disentanglement in variational autoencoders, *Advances in neural information processing systems* 31 (2018).
- [20] A. Kumar, P. Sattigeri, A. Balakrishnan, Variational inference of disentangled latent concepts from unlabeled observations, *arXiv preprint arXiv:1711.00848* (2017).
- [21] M. Kim, Y. Wang, P. Sahu, V. Pavlovic, Relevance factor vae: Learning and identifying disentangled factors, *arXiv preprint arXiv:1902.01568* (2019).
- [22] E. Dupont, Learning disentangled joint continuous and discrete representations, *Advances in Neural Information Processing Systems* 31 (2018).
- [23] F. Träuble, E. Creager, N. Kilbertus, F. Locatello, A. Dittadi, A. Goyal, B. Schölkopf, S. Bauer, On disentangled representations learned from correlated data, in: *International Conference on Machine Learning*, PMLR, 2021, pp. 10401–10412.
- [24] X. Shen, F. Liu, H. Dong, Q. Lian, Z. Chen, T. Zhang, Weakly supervised disentangled generative causal representation learning, *Journal of Machine Learning Research* 23 (2022) 1–55.
- [25] M. Yang, F. Liu, Z. Chen, X. Shen, J. Hao, J. Wang, Causalvae: Disentangled representation learning via neural structural causal models, in: *Proceedings of the IEEE/CVF conference on computer vision and pattern recognition*, 2021, pp. 9593–9602.
- [26] R. Suter, D. Miladinovic, B. Schölkopf, S. Bauer, Robustly disentangled causal mechanisms: Validating deep representations for interventional robustness, in: *International Conference on Machine Learning*, PMLR, 2019, pp. 6056–6065.
- [27] A. G. Reddy, V. N. Balasubramanian, et al., On causally disentangled representations, in: *Proceedings of the AAAI Conference on Artificial Intelligence*, 2022, pp. 8089–8097.
- [28] S. An, K. Song, J.-J. Jeon, Causally disentangled generative variational autoencoder, *arXiv preprint arXiv:2302.11737* (2023).
- [29] J. Brehmer, P. De Haan, P. Lippe, T. S. Cohen, Weakly supervised causal representation learning, *Advances in Neural Information Processing Systems* 35 (2022) 38319–38331.
- [30] S. Buchholz, G. Rajendran, E. Rosenfeld, B. Aragam, B. Schölkopf, P. Ravikumar, Learning linear causal representations from interventions under general nonlinear mixing, *arXiv preprint arXiv:2306.02235* (2023).
- [31] P. Lippe, S. Magliacane, S. Löwe, Y. M. Asano, T. Cohen, S. Gavves, Citris: Causal identifiability from temporal intervened sequences, in: *International Conference on Machine Learning*, PMLR, 2022, pp. 13557–13603.
- [32] A. Seigal, C. Squires, C. Uhler, Linear causal disentanglement via interventions, *arXiv preprint arXiv:2211.16467* (2022).
- [33] G. Papamakarios, E. Nalisnick, D. J. Rezende, S. Mohamed, B. Lakshminarayanan, Normalizing flows for probabilistic modeling and inference, *The Journal of Machine Learning Research* 22 (2021) 2617–2680.
- [34] D. Rezende, S. Mohamed, Variational inference with normalizing flows, in: *International conference on machine learning*, PMLR, 2015, pp. 1530–1538.
- [35] C.-W. Huang, D. Krueger, A. Lacoste, A. Courville, Neural autoregressive flows, in: *International Conference on Machine Learning*, PMLR, 2018, pp. 2078–2087.
- [36] D. P. Kingma, T. Salimans, R. Jozefowicz, X. Chen, I. Sutskever, M. Welling, Improved variational inference with inverse autoregressive flow, *Advances in neural information processing systems* 29 (2016).

- [37] I. Khemakhem, R. Monti, R. Leech, A. Hyvarinen, Causal autoregressive flows, in: International conference on artificial intelligence and statistics, PMLR, 2021, pp. 3520–3528.
- [38] A. Wehenkel, G. Louppe, Graphical normalizing flows, in: International Conference on Artificial Intelligence and Statistics, PMLR, 2021, pp. 37–45.
- [39] C. K. Sønderby, T. Raiko, L. Maaløe, S. K. Sønderby, O. Winther, Ladder variational autoencoders, *Advances in neural information processing systems* 29 (2016).
- [40] H. Hosoya, Group-based learning of disentangled representations with generalizability for novel contents, *arXiv preprint arXiv:1809.02383* (2018).
- [41] D. Bouchacourt, R. Tomioka, S. Nowozin, Multi-level variational autoencoder: Learning disentangled representations from grouped observations, in: Proceedings of the AAAI Conference on Artificial Intelligence, volume 32(1), 2018.
- [42] R. Shu, Y. Chen, A. Kumar, S. Ermon, B. Poole, Weakly supervised disentanglement with guarantees, *arXiv preprint arXiv:1910.09772* (2019).
- [43] F. Locatello, B. Poole, G. Rätsch, B. Schölkopf, O. Bachem, M. Tschannen, Weakly-supervised disentanglement without compromises, in: International Conference on Machine Learning, PMLR, 2020, pp. 6348–6359.
- [44] I. Khemakhem, D. Kingma, R. Monti, A. Hyvarinen, Variational autoencoders and nonlinear ica: A unifying framework, in: International Conference on Artificial Intelligence and Statistics, PMLR, 2020, pp. 2207–2217.
- [45] B. Schölkopf, Causality for machine learning, in: Probabilistic and Causal Inference: The Works of Judea Pearl, 2022, pp. 765–804.
- [46] J. He, Y. Gong, J. Marino, G. Mori, A. Lehrmann, Variational autoencoders with jointly optimized latent dependency structure, in: International conference on learning representations, 2018.
- [47] M. Kocaoglu, C. Snyder, A. G. Dimakis, S. Vishwanath, Causalgan: Learning causal implicit generative models with adversarial training, *arXiv preprint arXiv:1709.02023* (2017).
- [48] A. Hyvarinen, H. Morioka, Unsupervised feature extraction by time-contrastive learning and nonlinear ica, *Advances in neural information processing systems* 29 (2016).
- [49] L. Pacchiardi, R. Dutta, Score matched neural exponential families for likelihood-free inference., *J. Mach. Learn. Res.* 23 (2022) 1–71.
- [50] Z. Liu, P. Luo, X. Wang, X. Tang, Deep learning face attributes in the wild, in: Proceedings of the IEEE international conference on computer vision, 2015, pp. 3730–3738.
- [51] J. Pearl, *Causality*, Cambridge university press, 2009.
- [52] J. Pearl, et al., *Models, reasoning and inference*, Cambridge, UK: CambridgeUniversityPress 19 (2000).
- [53] I. Khemakhem, R. Monti, D. Kingma, A. Hyvarinen, Ice-beem: Identifiable conditional energy-based deep models based on nonlinear ica, *Advances in Neural Information Processing Systems* 33 (2020) 12768–12778.
- [54] C. Eastwood, C. K. Williams, A framework for the quantitative evaluation of disentangled representations, in: International conference on learning representations, 2018.

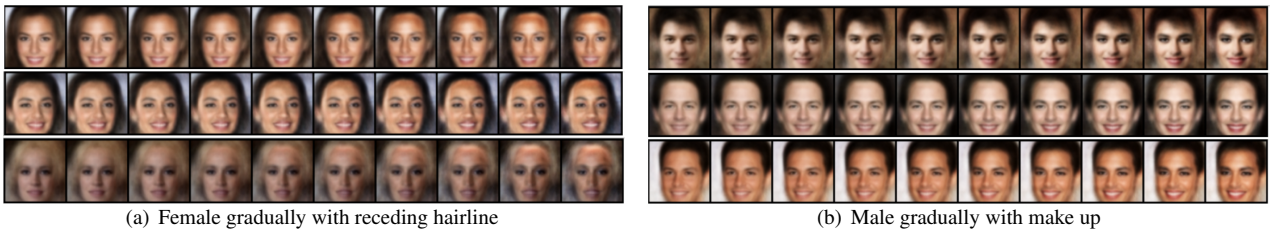


Figure C.1: Sample from interventional distributions.

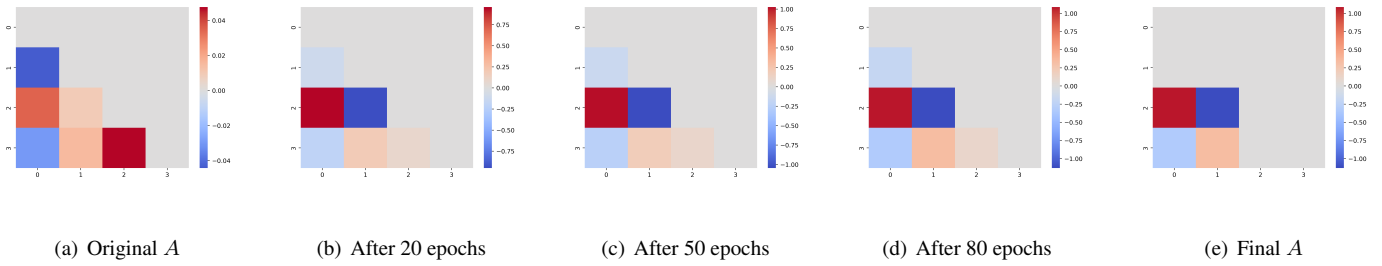


Figure C.2: The learned weighted adjacency matrix  $A$  given the causal ordering on Pendulum. (a)-(d) illustrate the changes in  $A$  as the training progresses. (e) represents  $A$  after edge pruning.

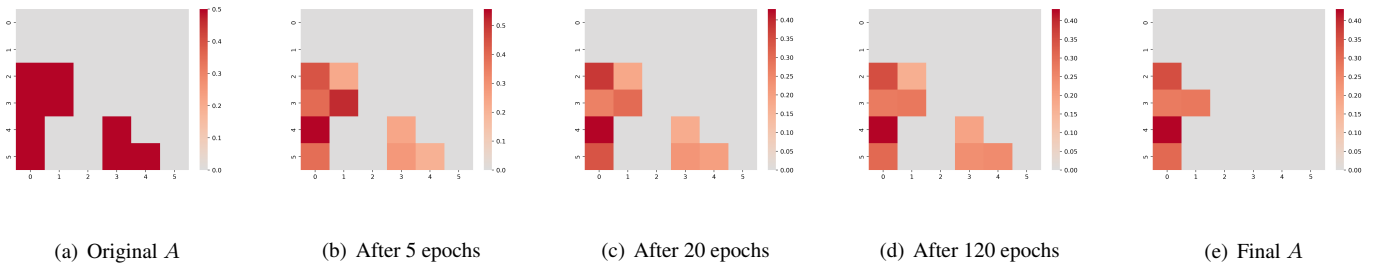
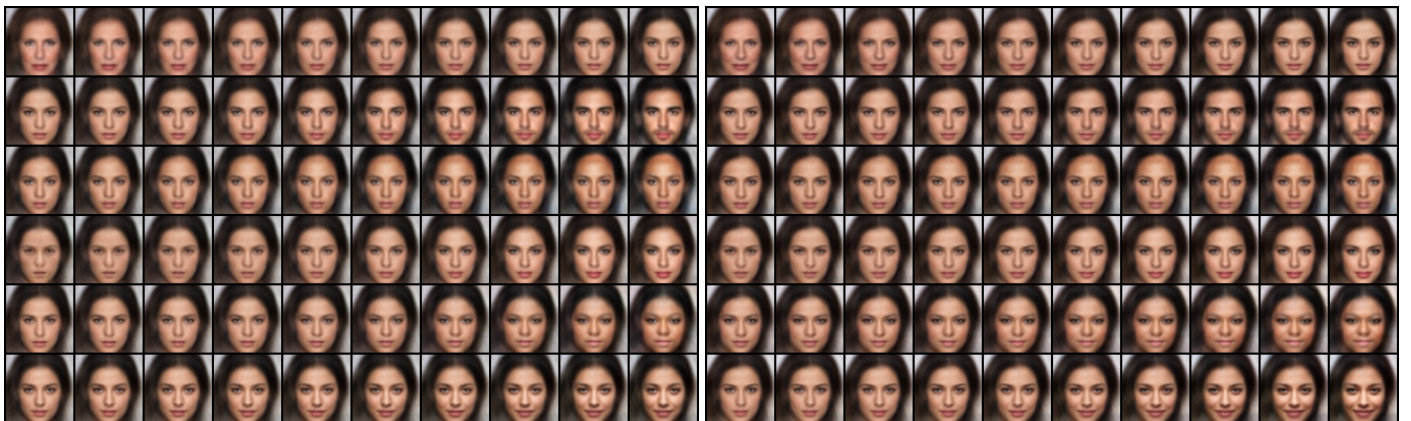


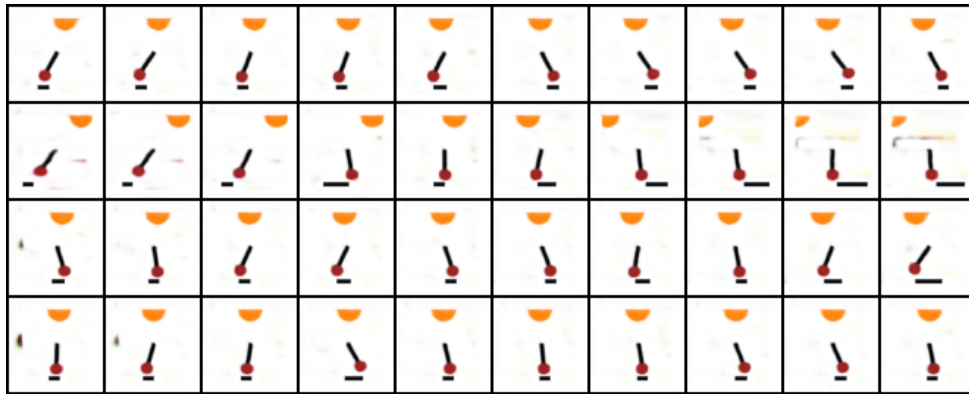
Figure C.3: The learned weighted adjacency matrix  $A$  given a super-graph on CelebA(Attractive). (a)-(d) illustrate the changes in  $A$  as the training progresses. (e) represents  $A$  after edge pruning.



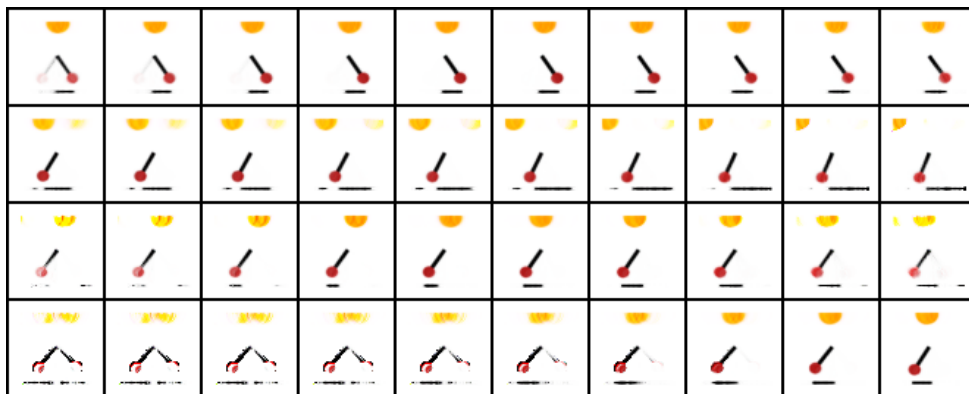
(a) Traverse of DCVAE on CelebA(Attractive)

(b) Intervention of DCVAE on CelebA(Attractive)

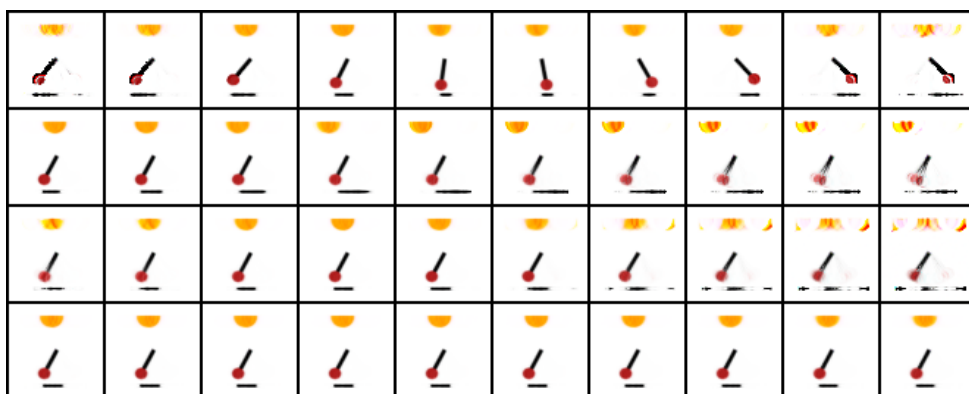
Figure C.4: Results of the DCVAE model under two types of interventions on CelebA(Attractive). Each row corresponds to one factor, in the same order as in Figure 2(b). We observe that our model achieves disentanglement, and when intervening on the causal variables, it affects the effect variables, while the opposite is not true.



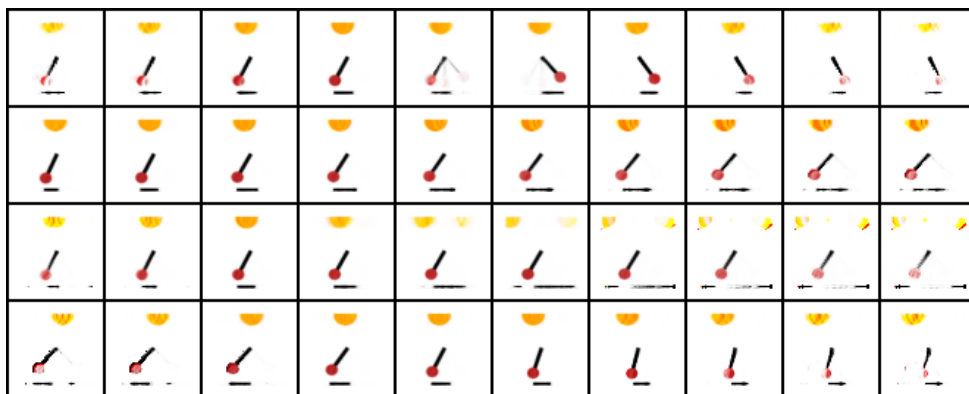
(a) DEAR



(b)  $\beta$ -VAE

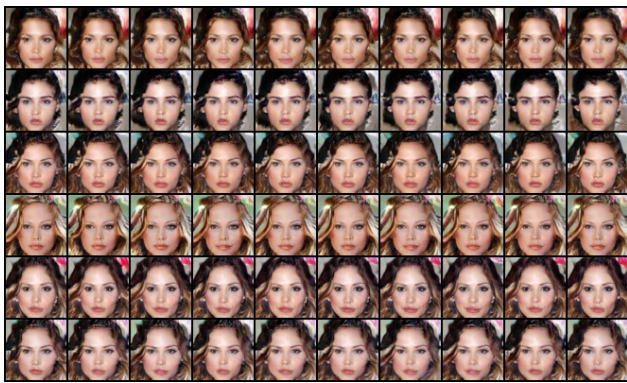


(c)  $\beta$ -TCVAE

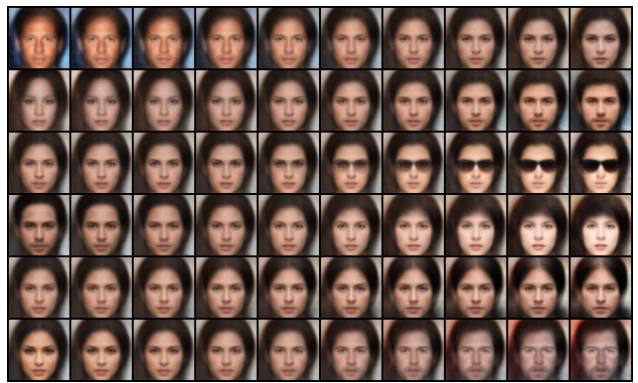


(d) VAE

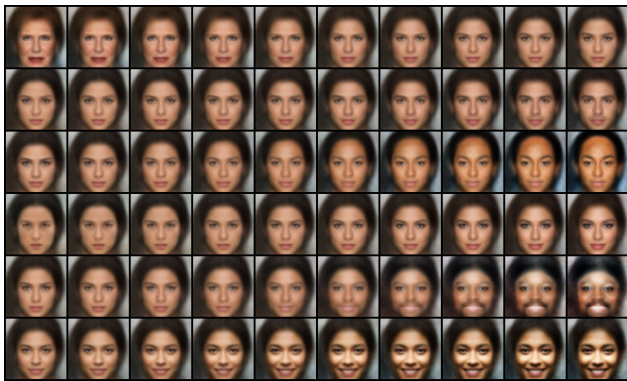
Figure C.5: Traverse results of four baseline models on Pendulum. We observe that changing one factor may result in changes in multiple factors, or no changes in any factor, such as the shadow length in the  $\beta$ -TCVAE. Therefore, their representations are all entangled on Pendulum.



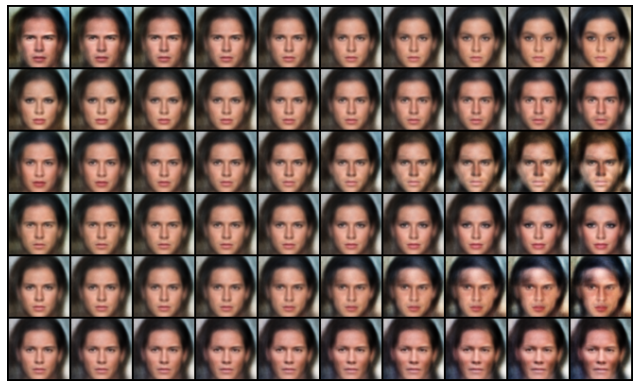
(a) DEAR



(b)  $\beta$ -VAE



(c)  $\beta$ -TCVAE

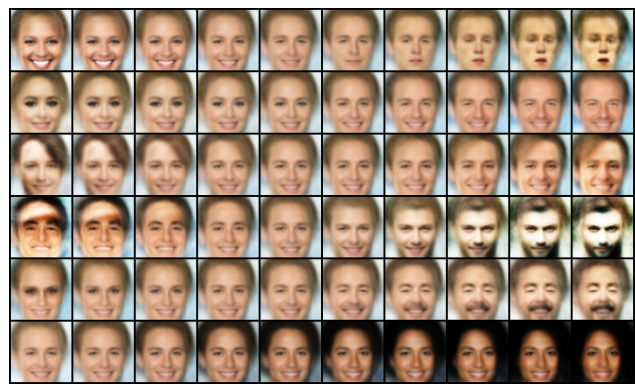


(d) VAE

Figure C.6: Traverse results of four baseline models on CelebA(Attractive).



(a) DEAR



(b)  $\beta$ -VAE



(c)  $\beta$ -TCVAE



(d) VAE

Figure C.7: Traverse results of four baseline models on CelebA(Smile).